Catalysis Today 161 (2011) 23–28

Contents lists available at ScienceDirect

Catalysis Today

journal homepage: www.elsevier.com/locate/cattod

Sulphur doped nanoparticles of TiO_2

Lórant Szatmáry[a,b,*], Snejana Bakardjieva[a], Jan Šubrt[a], Petr Bezdička[a], Jaromír Jirkovský[b], Zdeněk Bastl[b], Vlasta Brezová[c], Michal Korenko[d]

[a] Institute of Inorganic Chemistry of the AS CR, v.v.i., 250 68 Husinec-Řež, Czech Republic
[b] J. Heyrovský Institute of Physical Chemistry AS CR, v.v.i., Dolejškova 3, 182 23 Prague 8, Czech Republic
[c] Institute of Physical Chemistry and Chemical Physics, Faculty of Chemical and Food Technology, Slovak University of Technology in Bratislava, Radlinského 9, 812 37 Bratislava, Slovakia
[d] Institute of Inorganic Chemistry, Slovak Academy of Sciences, Dúbravska Cesta 9, 845 36 Bratislava, Slovakia

ARTICLE INFO

Article history:
Received 21 June 2010
Received in revised form
29 November 2010
Accepted 30 November 2010
Available online 11 January 2011

Keywords:
Photocatalyst
S-doped TiO_2
Thiourea
Visible light

ABSTRACT

Sulphur doped nanoparticles of titanium dioxide were prepared by the reaction of titanium butoxide and thiourea in methanol. X-ray powder diffraction and High resolution transmission electron microscopy were used to investigate the crystallinity of the prepared nanoparticles. Based on the X-ray photoelectron spectroscopy measurements sulphur is present in the form of S^{6+} which substitutes Ti^{4+} in the titania lattice. The band gap energies of synthesised photocatalyst were calculated from the fitting of experimental dependences by double Boltzmann symmetrical functions. The photocatalytic activity of the samples was determinated by the measurement of the 4-chlorophenol (4-CP) degradation in the aqueous suspensions in the ultraviolet and visible region. Electron paramagnetic resonance spectroscopy confirmed the generation of $^{\bullet}OH$ radicals from S doped TiO_2 under vis and UV irradiation.

1. Introduction

Titanium dioxide (TiO_2) is well-known as a photocatalyst for the photochemical applications because of its functionality, longterm stability and non-toxicity. However, TiO_2 is active only under ultraviolet (UV) light because of its large band gap energy and the solar energy contains only about 4% of UV light. There have been a lot of methods how to modify TiO_2 to extend the absorption to the visible area. Several authors substituted Ti^{4+} in TiO_2 by metal ion implantation (e.g., Cr^{3+} or V^{3+}, lanthanides, etc.) [1–3]. Nonmetal doping with S [4–6], N [7,8] and C [9,10] is also usually used for the photocatalytic applications in the visible region.

Umebayashi et al. proposed that the substitution of S for O (anionic doping) causes a significant red-shift of the absorption edge. Based on the ab initio band calculation the band gap narrowing originates from mixing the S 3p states with valence band leading to a rise in the valence band (VB) [6]. An alternative way is based on opinion how the dopant atom orbitals generate an isolated mid-gap level above the valence band [11,12]. The role of isolated mid-gap level holes is less clear, though they also should result in low energy "hole traps" that were less chemically active than the main valence band holes. Excitation in the low energy edge of the absorption would presumably mean direct formation of such trapped holes, but UV excitation could also lead to low energy trapped holes via migration to the dopant center [13]. Whether it is cationic or anionic, the doping of a foreign element into TiO_2 makes a donor or an acceptor level in the forbidden band and this level induces absorption of visible light. At the same time, however, this level may work as a carrier-recombination center, which decreases photocatalytic activity. Therefore, doping of a foreign element does not necessarily enhance response to visible light. To develop and improve visible-light-responsive photocatalysts, we should clarify what kind of doping or modification of TiO_2 is really effective in increasing photoactivity under visible light [14]. In the present work, TiO_2 powders doped with sulphur (S) were prepared by mixing titanium butoxide and thiourea in methanol. The nanoparticles prepared by this way were characterized by following methods: X-ray powder diffraction (XRD), high resolution transmission electron microscopy (HRTEM), UV–vis spectroscopy, EPR spectroscopy, X-ray photoelectron spectroscopy (XPS). The photocatalytic activity of the samples was determined by the measurement of the 4-CP degradation in the aqueous suspensions in the ultraviolet and visible region.

* Corresponding author at: Institute of Inorganic Chemistry of the AS CR, v.v.i., 250 68 Husinec-Řež, Czech Republic. Tel.: +420 2 6617 2190; fax: +420 2 2094 1502.
E-mail address: szatmary@iic.cas.cz (L. Szatmáry).

0920-5861/$ – see front matter © 2010 Elsevier B.V. All rights reserved.
doi:10.1016/j.cattod.2010.11.082

2. Methods

2.1. Chemicals and reagents

Titanium butoxide (99%, Aldrich), thiourea (Lachema, Czech Republic), methanol (99%, LiChrosolv Merck) and 4-CP (99%, Fluka) were used as received. The spin trapping agent, 5,5-dimethyl-1-pyrroline *N*-oxide (DMPO, Aldrich) was freshly distilled before application and stored under argon at −18 °C. The concentration of photogenerated adducts was determined using aqueous solutions of 4-hydroxy-2,2,6,6 tetramethylpiperidine *N*-oxyl (TEMPOL; Aldrich) as calibration standards measured under strictly identical EPR instrument settings.

2.2. Catalyst preparation

Two solutions were prepared. First solution contained 60 mL of titanium butoxide dissolved in 250 mL methanol. Second solution contained 64 g of thiourea dissolved in 250 mL methanol. Solutions 1 and 2 were mixed together with magnetic stirrer at room temperature and after evaporation of methanol white powder was obtained. The white powder (TiS) was then calcinated at 400 (TiS-400), 500 (TiS-500), 600 (TiS-600) and 700 °C (TiS-700) for 3 h (heating rate 5 °C/min).

2.3. Characterization of the catalysts

Diffraction patterns were collected using a PANalytical X'Pert PRO diffractometer equipped with a conventional X-ray tube (CuK_α 40 kV, 30 mA, line focus) in transmission mode, an elliptic focusing mirror, a divergence slit 0.5°, an anti-scatter slit 0.5° and a Soller slit of 0.02 rad were used in the primary beam. A fast linear position sensitive detector PIXcel with an anti-scatter shield and a Soller slit of 0.02 rad were used in the diffracted beam. All patterns were collected in the range of 18–88°. 2θ with the step of 0.013° and 250 s/step.

Starting sample TiS was studied by in situ heating in air on a PANalytical X'Pert PRO diffractometer using $Co_{K\alpha}$ radiation (40 kV, 30 mA) and a multichannel detector X'Celerator with an anti-scatter shield, equipped with a high temperature chamber (HTK 16, Anton Paar, Graz, Austria). The measurement started at room temperature and finished at 1000 °C with a step of 25 °C from 550 to 1000 °C (step of 100 °C in the remaining ranges). Desired temperature was reached by a heating rate of 60 °C/min and held while collecting data. A diffraction pattern was acquired from 19° to 93° 2θ in a step-scan mode (step 0.017°, acquisition time 18 min) at each temperature.

Qualitative analysis was performed with HighScorePlus software package (PANalytical, the Netherlands, version 2.2.5), Diffrac-Plus software package (Bruker AXS, Germany, version 8.0) and JCPDS PDF-2 database [15]. For quantitative analysis of XRD patterns we used Diffrac-Plus Topas (Bruker AXS, Germany, version 4.2) with structural models based on ICSD database [16]. This program permits to estimate the weight fractions of crystalline phases by means of Rietveld refinement procedure.

Transmission electron micrographs were obtained using a JEOL JEM 3010 microscope operating at accelerating voltage of 300 kV. The samples for electron microscopy were prepared using grinding and dispersing the powder in propanol and applying a drop of very dilute suspension on carbon coated grids. The suspensions were dried by slow evaporation at ambient temperature.

The diffuse reflectance spectra of the powder photocatalysts placed in a 5 mm quartz cell were measured using the Lambda 19 UV/VIS/NIR spectrophotometer (PerkinElmer) equipped with an integrating sphere. The original coordinates of the spectra (reflectance vs. wavelength) were transformed to Kubelka–Munk function (K) vs. photon energy ($h\nu$) [17]. The values of the band gap energy are usually estimated by extrapolation of the linear part of the dependence [18]. However, we employed a more precise method based on the fitting of experimental dependences by double Boltzmann symmetrical functions by means of nonlinear regression. Then the calculated crossing point of the tangent line in the inflection point of the Boltzmann fit with its lower asymptote determines the energy band gap energy. The same procedure applying the fitting with single Boltzmann symmetrical function is described in [19]. For the powders composed of more components (e.g., two different crystallographic phases), the single Boltzmann function did not fit the experimental data well. In such cases, a double Boltzmann function fit by a sum of two Boltzmann functions was applied.

X-ray photoelectron spectra were measured on a VG ESCA 3 Mk II spectrometer using Al Kα radiation. The spectrometer was operated in the fixed analyzer transmission mode using 20 eV pass energy. The background pressure during the spectra accumulation was typically 10^{-7} Pa. The samples were spread on gold substrate. Detailed spectral scans were taken over Ti 2p, O 1s, S 2p and C 1s regions. Core-level binding energies were determined with an accuracy of ±0.2 eV. Quantification of element concentration ratios was accomplished by correcting the photoelectron peak areas for their cross-sections and accounting for the dependence of electron inelastic mean free path on the kinetic energy [20]. Spectra fitting was carried out using nonlinear background and the lines of Gaussian–Lorentzian shape.

The formation of hydroxyl radicals upon irradiation of TiO_2 aqueous suspensions was investigated by EPR spin trapping technique using DMPO. The instantly prepared TiO_2 suspensions containing DMPO were carefully mixed by slight air stream and immediately transferred to a quartz flat cell (WG 808-Q, Wilmad-LabGlass, USA) optimized for the TE102 cavity. The samples were irradiated at 295 K directly in the EPR resonator, and EPR spectra were recorded in situ using EMX X-band EPR spectrometer (Bruker, Germany). As an irradiation source an HPA 400/30S lamp (400 W, Philips) was used. The radiation flux was focused to obtain high intensity in the active part of TE102 cavity. UVA lamp irradiance of 2.7 mW cm^{-2} inside the EPR cavity was determined using a UV Light Meter UV-340 (Lutron Ltd., UK). A Pyrex glass filter (with thickness of 1 mm) was applied to eliminate radiation wavelengths below 300 nm. A GG 435 filter (Schott Glaswerke, Germany) was used to cut off wavelengths shorter than 420 nm. The stock suspensions were prepared by dispersing 10 mg TiO_2 powder in 10 mL distilled water, and then carefully homogenized in an ultrasound bath (60 s, Ultrasonic Compact Cleaner TESON 1, Tesla, Slovak Republic) before use. The concentration of the DMPO stock solutions was 0.2 mol L^{-1}. The experimental EPR spectra acquisition, integration and their simulations were carried out using WIN EPR and SimFonia standard programs (Bruker).

The photocatalytic decomposition of 4-CP was carried out in a self-constructed photo reactor [21]. Two light sources were used, TESLA 125 W Black lamp to determine the activity in the UV region and the NARWA 400 W Blue Lamp to determine the visible light activity.

3. Results and discussion

The crystalline phases of the S doped TiO_2 nanopowders were analyzed by X-ray diffraction. Fig. 1 shows the XRD patterns of sulphur doped photocatalysts prepared at various temperatures. The properties of the prepared photocatalysts are summarised in Table 1. As shown in Fig. 1, the crystalline phase of calcinated S doped photocatalyst was pure anatase (ICDD PDF card 21-1272) in the temperature range 400–600 °C. The sample prepared at 400 °C

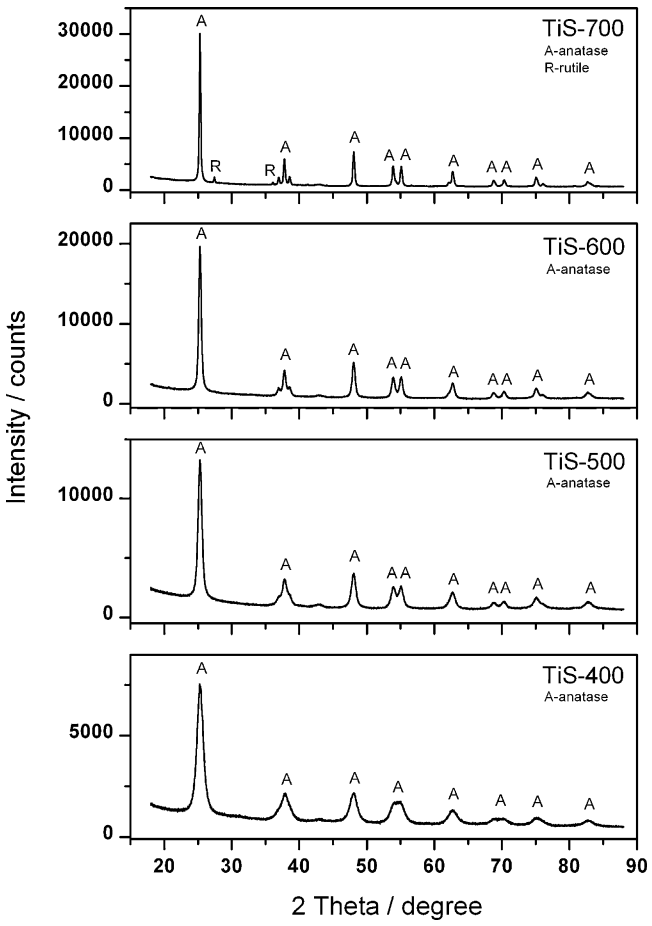

Fig. 1. XRD patterns of S doped TiO_2 powders prepared by different calcination temperatures.

shows a significant line broadening which reflects fine crystallite size. The crystallite size of anatase (9 nm) increases with the increase of the temperature to 25 nm (600 °C). Anatase crystalline structure is stable up to 700 °C. This stabilization of anatase phase could be explained by taking into account the presence of sulphate groups (from decomposition of thiourea) anchored on the TiO_2. Thus, the impregnated sulphate ions seem to delay anatase to rutile transformation, stabilizing anatase structure [22]. The sample heated at 700 °C contained besides anatase also rutile phase (ICDD PDF card 21-1276).

Three phases were observed during in situ heating XRD experiment: thiourea, anatase and rutile (Fig. 2). No diffraction lines of sulphur or other phases were observed, which means that all S is incorporated into the TiO_2 structure. Thiourea is present up to 100 °C, above this temperature the system gets amorfized. Anatase starts to crystallize at 500 °C and is the predominant main phase up

Table 1
Structural and optical characterization of the TiS samples.

Sample	Structural parameters of anatase			Band gap	
	Crystallite size (nm)	a/Å	c/Å	Sulphur phase (E_{g1}/eV)	Anatase phase (E_{g2}/eV)
TiS-400	9.1	3.7871	9.5025	2.27	3.21
TiS-500	15.5	3.7867	9.5086	2.27	3.18
TiS-600	24.9	3.7857	9.5133	2.31	3.13
TiS-700	50.6	3.7841	9.5157	–[a]	3.07

[a] Single Boltzmann fit.

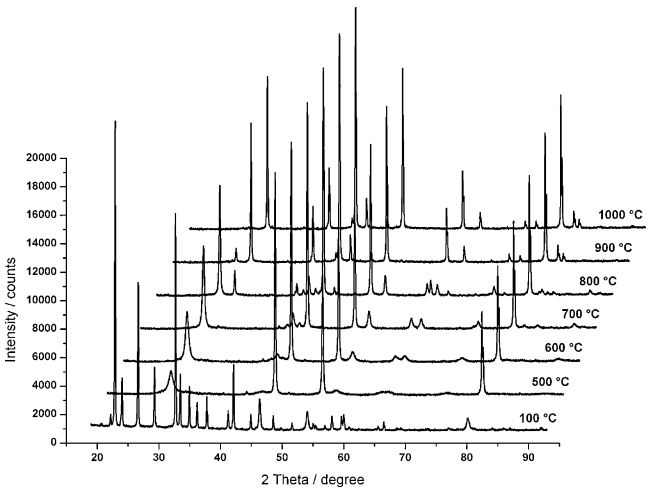

Fig. 2. In situ XRD patterns of the starting sample TiS.

to 700 °C. Above this temperature two phases are present, anatase and rutile. These results are in agreement with Colón et al. [22] who observed anatase to rutile transition around 700 °C. Sulphur doped TiO_2 photocatalyst completes the transformation to rutile at 975 °C.

The S doped TiO_2 samples prepared at 400 and 700 °C were observed by high resolution transmission electron microscopy. The sample prepared at 400 °C is formed by 8–10 nm crystals embedded in amorphous material (see Fig. 3a). The crystallite size and morphology of the nanopowders obtained after the calcination at 700 °C can be seen in Fig. 4. The photocatalyst prepared at 700 °C contains two phases, anatase and rutile. The size of anatase and rutile particles is in range 50–60 nm. The size of the nanocrystallites calculated from the width of XRD diffraction is in good agreement with the crystallite size determined from HRTEM observation.

Diffuse reflectance spectra of the sulphur doped photocatalysts have two characteristic spectral components with different properties. While the electronic structure of TiO_2 shows a typical semiconductor absorption with the spectral edge in UV region, the sulphur doping causes light absorption in visible range. The intensity of the yellow color of the samples depends on the temperature of the calcination, thus of the amount of sulphur in the samples. Fig. 5 shows the UV–vis diffuse reflectance spectra of the S-doped powders. The samples prepared at 400 and 500 °C showed a strong absorption in the visible region. With the increase of the temperature of calcination above 500 °C, the absorption in the visible region decreases gradually and the sample prepared at 700 °C has the absorption edge shifted to the UV region (Fig. 5).

In Table 1 are shown calculated values of band gap energies of the samples from the double Boltzmann function fitting. For each sample it has been calculated the Eg for the region of sulphur doping (Eg1) and for the anatase phase (Eg2). The value of Eg1 for the sample TiS-400 equals the value for the sample TiS-500 (2.27 eV, 546 nm) because the shape of the curves in the region 3.2–2.3 eV is approximately identical. Bayati et al. [23] have calculated the similar bang gap energy (2.29 eV) for sulphur doped TiO_2 layers. The values of Eg2 differ from each other (3.21 eV and 3.18 eV), but they are in the match with the value for the pure anatase TiO_2 (3.23 eV, 385 nm). With the increase of the temperature of calcination above 600 °C, the band gap energy for the region of sulphur doping (Eg1) equals 2.31 eV, respectively 537 nm (Fig. 6).

The overall surface stoichiometry calculated from integrated intensities of individual spectral peaks measured in the high resolution mode is $TiO_{2.56}S_{0.13}C_{0.54}$ (TiS-400), $TiO_{2.46}S_{0.083}C_{0.39}$ (TiS-500), $TiO_{2.39}S_{0.068}C_{0.42}$ (TiS-600) and $TiO_{2.29}S_{0.029}C_{0.50}$ (TiS-700).

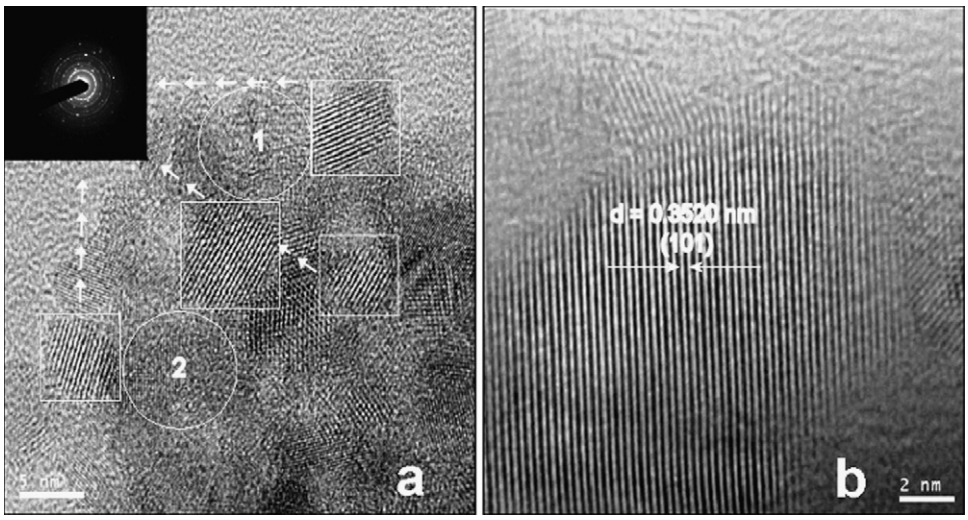

Fig. 3. HRTEM images of catalyst TiS-400: (a) with amorphous domains (1, 2), inserted is an electron diffraction pattern of anatase, and (b) high resolution picture of anatase nanocrystal.

Titanium is present in all samples as Ti^{4+} ion with a binding energy of Ti 2p3/2 electrons equal to 459.1 ± 0.2 eV. With increasing of the calcination temperature binding energy of Ti 2p and O 1s electrons decreases, the energies of the samples heated at 700 °C are shifted by 0.4 eV towards lower values. This may be caused by the shift in the Fermi level towards the upper edge of the valence band.

The photoelectron spectra of O 1s electrons show presence of the two different chemical states of oxygen, lattice oxygen (530.3 eV) and oxygen in surface hydroxyl groups or C–O bonds (532.1 eV).

Sulphur is present in all samples in a single chemical state with binding energy of S 2p3/2 electrons equal to 168.7 ± 0.2 eV (Fig. 7). This value is consistent with values reported in the literature (http://srdata.nist.gov/xps/index.htm) for hexavalent sulphur S^{6+} [4]. With increasing temperature of thermal treatment the concentration of sulphur in the samples decreases. No peak corresponding to S^{2-} state (160–161 eV) was observed. These results show that the sulphur ions occupy the Ti^{4+} sites, however, the main part of the sulphur content is adsorbed on the surface in the form of sulphate ions.

The spectrum of C 1s photoelectrons was dominated by peak located at 284.4 eV. The same peak we observed also with pure, undoped anatase sample and assigned it to adventitious carbon. Adsorption of atmospheric hydrocarbons onto surfaces prepared in the typical laboratory environment is known to result in the presence of a C 1s signal the intensity of which is related to the amount of carbonaceous species. For carbon doped titania the C 1s peak was observed at about 282 eV [9,24], that is at lower binding energy than we measured for our samples. Let us to mention that formation of carbonates was also discussed as responsible for narrowing of the titania band gap [25]. Two kinds of carbonate species were observed by the authors with binding energies of C 1s electrons 287.5 and 288.5 eV, that is at much higher binding energy than we obtained for our samples. Consequently, we do not expect the carbon species will act in our samples as a dopant.

Upon UVA irradiation of aerated TiO_2 suspensions in the presence of DMPO, typical four-line EPR spectra were monitored, characterized by spin Hamiltonian parameters a_N = 1.495 mT, a_H^β = 1.472 mT; g = 2.0057, attributed to the hydroxyl radical added to DMPO (•DMPO-OH), as is shown in the inset of Fig. 8. Upon UV irradiation of all S doped TiO_2 samples the generation of •DMPO-

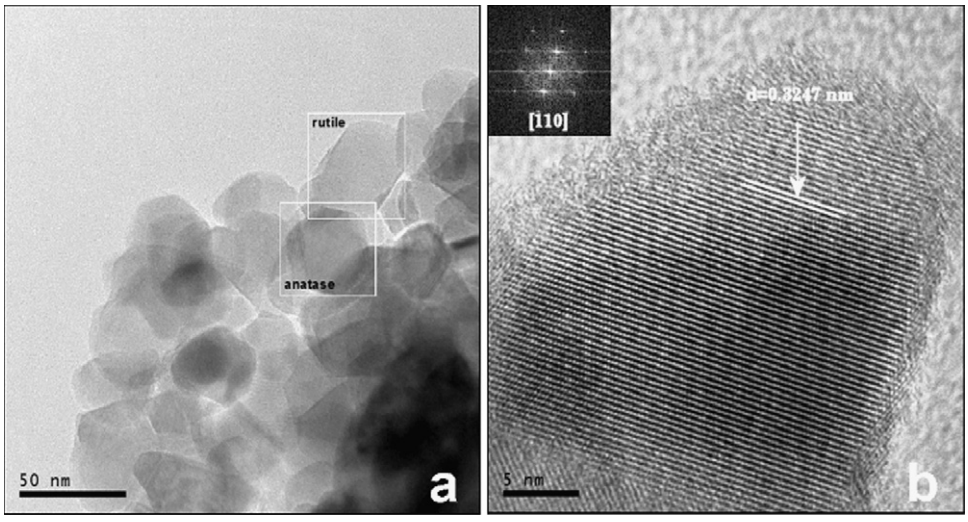

Fig. 4. HRTEM images of catalyst TiS-700: (a) low magnification image of nanocrystalline powder, and (b) high resolution picture of rutile nanocrystal, corresponding electron diffraction pattern of rutile is inserted.

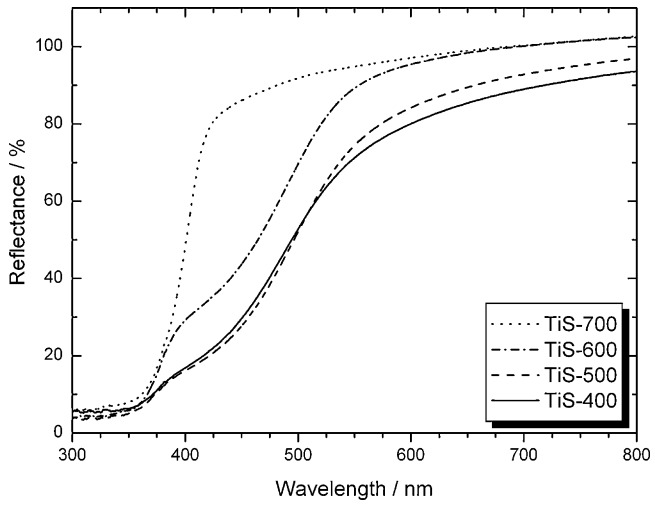

Fig. 5. UV–vis diffuse reflectance spectra of S doped TiO_2 photocatalysts.

OH was evidenced. Photoexcitation using visible light ($\lambda > 420$ nm) resulted in the significant lowering of EPR signal intensity of •DMPO-OH, consequently, higher exposures were necessary to obtain EPR spectra with adequate signal-to-noise ratio (Fig. 8). However, the quantitative evaluations of photoinduced generation of •DMPO-OH upon UV or vis irradiation require quantum yield or quantum efficiency calculation [26]. It should be noted here, that the paramagnetic signals of •DMPO-OH may be produced directly by the addition of photoproduced hydroxyl radicals, but we cannot exclude an alternative mechanism assuming spin trap oxidation by photogenerated holes to radical cation $DMPO^{\bullet+}$, which hydrolyses in the aqueous media to •DMPO-OH without direct hydroxyl radical formation [27,28].

The effect of sulphur doping of titania in the processes of aromatics decomposition was recently deeply discussed by Rockafellow et al., assuming the role of sulphur doping sites as deep hole traps that diminish the oxidizing power of the hole and inhibit the hydroxyl radical generation [13].

The sample prepared at 400 °C showed the slowest photodecomposition of 4-CP under UV irradiation (Fig. 9). It could be explained by small particle size and high content of amorphous phase in this sample. Photoactivity of the samples prepared at 600 °C and 700 °C was almost identical. The photocatalysts calcinated between 400 and 600 °C were yellowish and that is why they were photoactive in visible region. The sample heated at 700 °C was white and no more photoactive under visible irradiation (Fig. 10).

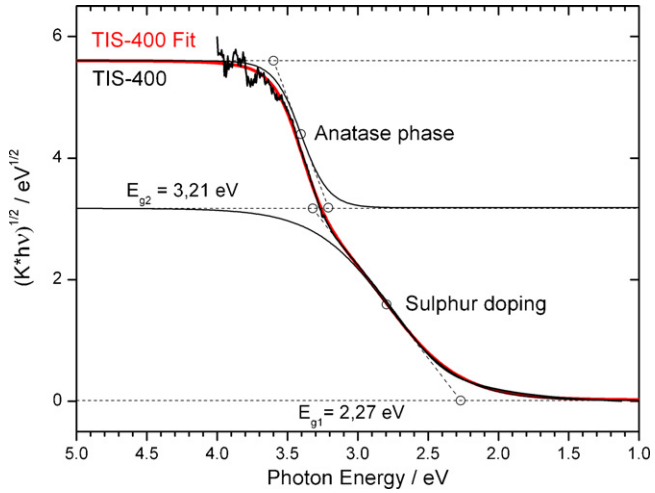

Fig. 6. Determination of band gap energy (sample TIS-400) from the transformed diffuse reflectance spectrum.

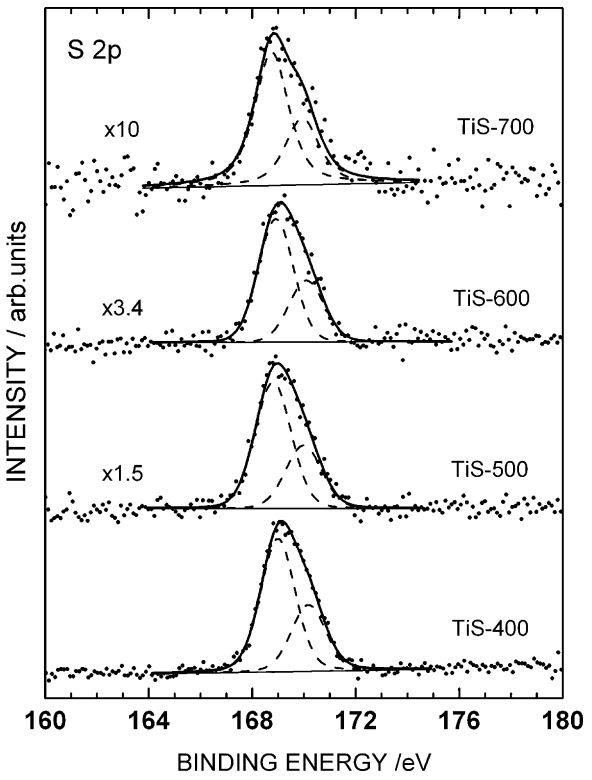

Fig. 7. XP spectra of S 2p electrons for TiS samples. Spectra were normalized to the same height by multiplying them by factor displayed on their left hand side.

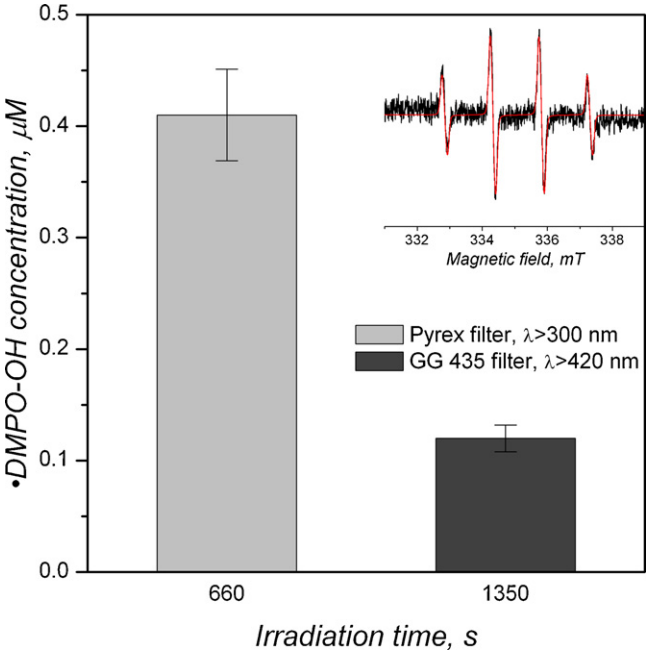

Fig. 8. Concentration of •DMPO-OH spin adduct monitored in aerated aqueous suspensions of TiS-500 upon UVA (■, $\lambda > 300$ nm) and vis (■, $\lambda > 420$ nm) irradiation in the presence of DMPO spin trap ($c_{TiS\text{-}500} = 0.875$ g L^{-1}, $c_{0,DMPO} = 0.025$ mol L^{-1}). Inset represents experimental (black line) and simulated (red line) EPR spectrum of •DMPO-OH adduct obtained after 660 s of UVA exposure. (For interpretation of the references to color in this figure legend, the reader is referred to the web version of the article.)

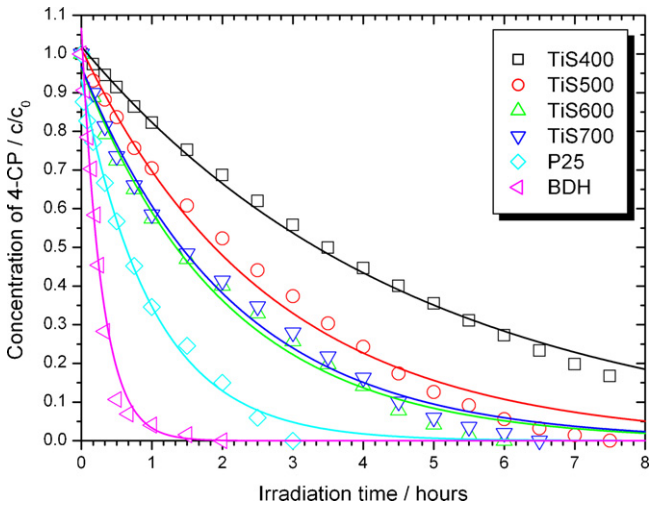

Fig. 9. Photoactivity of TiS photocatalysts under UV light.

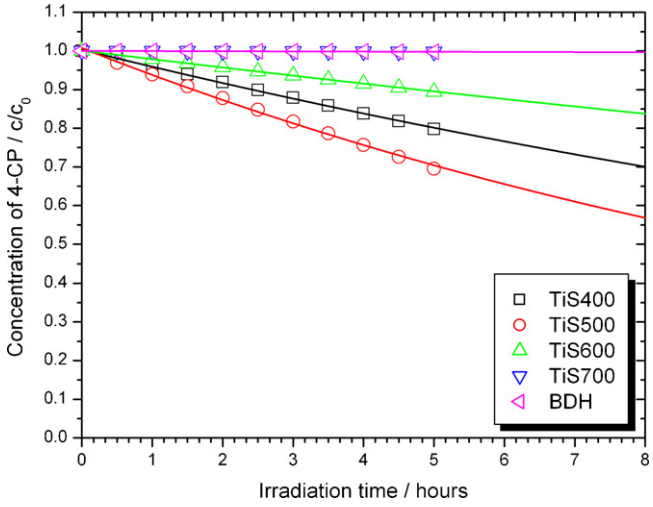

Fig. 10. Photoactivity of TiS photocatalysts under visible light.

4. Conclusions

S doped nanoparticles of TiO_2 were prepared by the reaction with titanium butoxide and thiourea. The band gap energies of synthesised photocatalyst were calculated from the fitting of experimental dependences by double Boltzmann symmetrical functions. It was found that the increase of the calcination temperature led to a decrease of the sulphur content. It caused a formal blue shift of the edge of corresponding diffuse reflectance spectra from visible to UV range. According to XPS spectroscopy sulphur is present in every sample just in one chemical state, thus hexavalent sulphur S^{6+}. Our EPR results confirmed the generation of $^{\bullet}OH$ radicals from S doped TiO_2 under vis and UV irradiation.

Acknowledgments

This work was supported by the Ministry of Education, Youth and Sports of the Czech Republic (project no lM4531477201) and Scientific Grant Agency of the Slovak Republic (project VEGA/1/0018/09).

References

[1] T. Kudo, Y. Kudo, A. Ruike, A. Hasegawa, M. Kitano, M. Anpo, Catal. Today 122 (2007) 14.
[2] Y. Cong, L. Xiao, J.L. Zhang, F. Chen, M. Anpo, Res. Chem. Intermed. 32 (2006) 717.
[3] M. Anpo, M. Takeuchi, J. Catal. 216 (2003) 505.
[4] T. Ohno, T. Mitsui, M. Matsumura, Chem. Lett. 32 (2003) 364–365.
[5] T. Ohno, M. Akiyoshi, T. Umebayashi, K. Asai, T. Mitsui, M. Matsumura, Appl. Catal. A 265 (2004) 115–121.
[6] T. Umebayashi, T. Yamaki, H. Itoh, K. Asai, Appl. Phys. Lett. 81 (2002) 454–456.
[7] K. Kobayakawa, Y. Murakami, Y. Sato, J. Photochem. Photobiol. A 170 (2004) 177–179.
[8] R. Asahi, T. Morikawa, T. Ohwaki, K. Aoki, Y. Taga, Science 293 (2001) 269–271.
[9] H. Irie, Y. Wanatabe, K. Hashimoto, Chem. Lett. 32 (2003) 772–773.
[10] M. Shen, Z. Wu, H. Huang, Y. Du, Z. Zou, P. Yang, Mater. Lett. 60 (2006) 693–697.
[11] H. Irie, Y. Watanabe, K. Hashimoto, J. Phys. Chem. B 107 (2003) 5483–5486.
[12] V.N. Kuznetsov, N. Serpone, J. Phys. Chem. B 110 (2006) 25203–25209.
[13] E.M. Rockafellow, L.K. Stewart, W.S. Jenks, Appl. Catal. B 91 (2009) 554.
[14] K. Takeshita, A. Yamakata, T. Ishibashi, H. Onishi, K. Nishijima, T. Ohno, J. Photochem. Photobiol. A 177 (2006) 269–270.
[15] JCPDS PDF-2 database, International Centre for Diffraction Data, Newtown Square, PA, U.S.A., release 54, 2004.
[16] ICSD database, FIZ Karlsruhe, Germany, release 2009/1, 2009.
[17] G.F. Kortüm, Reflectance Spectroscopy: Principles, Methods, Applications, Springer-Verlag, New York, 1969.
[18] A Blažková, I. Csölleová, V. Brezová, J. Photochem. Photobiol. A 113 (1998) 253.
[19] K. Kočí, L. Obalová, L. Matějová, D. Plachá, Z. Lacný, J. Jirkovský, O. Šolcová, Appl. Catal. B 89 (2009) 496.
[20] J. Powell, A. Jablonski, NIST Electron Inelastic-Mean-Free-Path Database, Version 1.1, U.S. Dept. of Commerce, NIST, Gaithersburg, MD, 2000.
[21] S. Bakardjieva, J. Subrt, V. Stengl, M.J. Dianez, M.J. Sayagues, Appl. Catal. B 58 (2005) 193.
[22] G. Colón, M.C. Hidalgo, G. Munuera, I. Ferino, M.G. Cutrufello, J.A. Navío, Appl. Catal. B 63 (2006) 45–59.
[23] M.R. Bayati, A.Z. Moshfegh, F.G. Fard, Appl. Catal. A 389 (2010) 60–67.
[24] C. Yeongsoo, T. Umebayashi, M. Yoshikawa, J. Mater. Sci. 39 (2004) 1837.
[25] Y. Li, D.S. Hwang, N.H. Lee, S.J. Kim, Chem. Phys. Lett. 404 (2005) 25.
[26] N. Serpone, A.V. Emeline, Int. J. Photoenergy 4 (2002) 93–131.
[27] Y. Nosaka, S. Komori, K. Yawata, T. Hirakawa, A. Nosaka, Phys. Chem. Chem. Phys. 5 (2003) 4731–4735.
[28] V. Brezová, D. Dvoranová, A. Staško, Res. Chem. Intermed. 33 (2007) 251–268.